Numerical modeling of the three-dimensional flows in the ground boundary layer of a maintained axisymmetrical vortex

By S. W. CHI, *The George Washington University, Washington, D.C.* and J. JIH, *COMSAT Laboratories, Clarksburg, Md.*

(Manuscript received June 12, 1973; revised version January 2, 1974)

ABSTRACT

The three-dimensional flow in the ground boundary-layer beneath an intense Rankine vortex is studied, using a numerical technique. Equations of motion in terms of dimensionless vorticity, stream function and circulation have been derived and generalized. Upwind instead of the usual central difference scheme has been used. The method was found to be stable for the range of Reynolds numbers for the natural tornado. The results predict the known physical characteristics of the three-dimensional boundarylayer of intense vortices, namely: The distribution of horizontal velocities in the vertical direction is oscillatory in the outer region; and the motion in the core region is upward, whilst there is weak descending motion in the outer region. The predicted pressure distribution also falls within the range observed for the natural tornado.

1. Introduction

The theoretical study of the boundary layers beneath intense atmospheric vortices such as tornadoes does not appear to have been well developed. The flow in these boundary layers will certainly be turbulent and even the assumption of uniform fluid viscosity still leads to considerable difficulty. The crux of the problem lies in nonlinearity of the boundary layer equations, and the rapid change of tangential velocity outside the bondary layer from a state of near solid rotation close to the axis of symmetry to a potential flow in the outer regions. The previous theoretical treatments have been limited either to the similar solutions for the vertical velocity distributions or to the solutions of momentum-integral equations by using assumed vertical distributions; when the tangential velocity for the outer flow is given by the power law:

$$v^{+} \propto 1/r^{n} \quad (1)$$

Bödewadt (1940) obtained a similar solution of the Navier-Stokes equations near the axis of symmetry when the outer flow is in solid-body rotation, $n = -1$; and Stewartson (1957) and Mack (1964) obtained similar solutions of the boundary-layer equations which are valid for the region near the edge of a finite disk. Solutions of the momentum-integral equations have been obtained by Schultz-Grunow (1935) for the case where the outer flow is in solid-body rotation, $n = -1$; and by Taylor (1950), Weber (1956), Anderson (1961), Mack (1962) and Rott & Lewellen (1964) for the case where the outer flow is in potential flow, $n = 1$. Because of the limitations of these approaches, it is rather difficult to apply their results to the boundary-layer flows of a real vortex where the motions in the various parts are mutually dependent and the vertical distributions also change from region to region.

In view of the fact that the full Navier-Stokes equations can now be solved economically with the aid of a high-speed computer. This paper represents an attempt to solve numerically the full equations governing the boundary-layer flow of an intense vortex which has a structure of a Rankine combined vortex, namely, one with a core of large vorticity and an outer region of zero vorticity. As a beginning only the uniform fluid property is considered; no other simplifying assumption will be made.

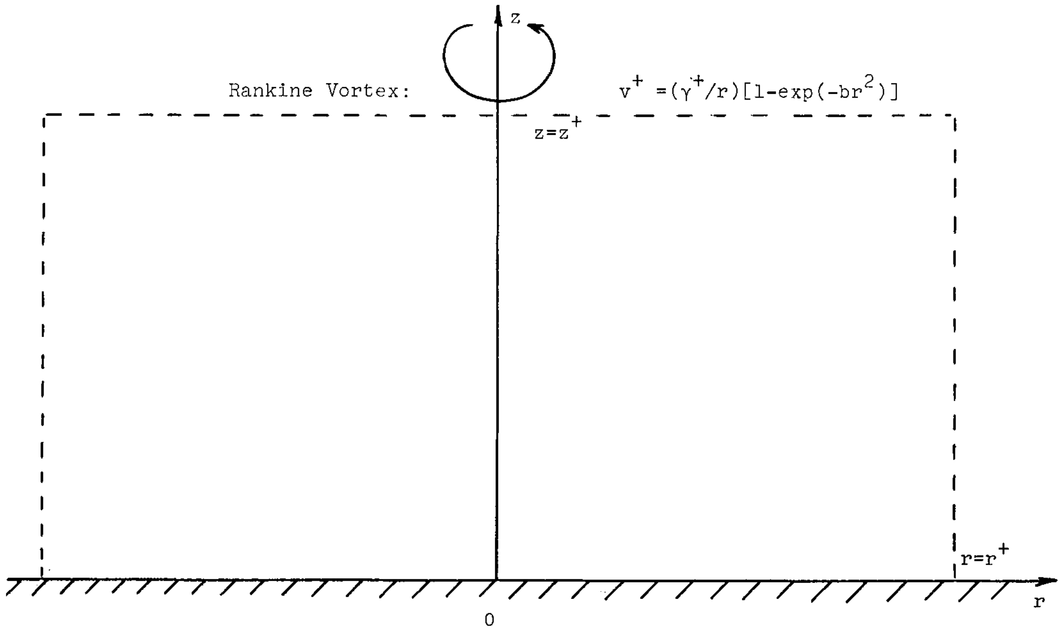

Fig. 1. Schematic representation of flow region under study.

In Section 2 below the governing equations in terms of dimensionless vorticity, stream function and circulation are derived and generalized. The appropriate boundary conditions for solving these equations are derived in Section 3. Developments of numerical procedure and computer program are described in Sections 4 and 5, respectively. Results of this work are presented and discussed in Section 6; and conclusions are given in Section 7.

2. Physical model and governing equations

The physical model illustrated in Fig. 1 was used as the basis for this study of the-boundary-layer-flow near the ground surface. Far above the ground at $z = z^+$, a two-dimensional Rankine vortex is maintained:

$$v^+ = (\gamma^+/r)[1 - \exp(-br^2)] \qquad (2)$$

where b is a constant defined as the reciprocal of square of a characteristic radius and γ^+ is another constant defined as the circulation v^+r at large radius. Numerical techniques are used to solve the equations of motion for incompressible fluid with uniform viscosity for the region enclosed by $0 < z < z^+$ and $0 < r < r^+$.

The following dimensionless variables are defined:

$$U = u/v_m, \quad V = v/v_m, \quad W = w/v_m,$$

$$P = p/(\varrho v_m^2), \quad R = r/r_m, \quad Z = z/r_m,$$

$$K = 1/N = \nu/(v_m r_m).$$

Where (u, v, w) are the velocity components in the cylindrical coordinate system (r, θ, z), p is the derivation from the hydrostatic pressure, ϱ the density, ν the coefficient of kinematic viscosity, v_m the maximum tangential velocity for the main vortex, r_m the radius at which $v = v_m$ and $N(=1/K)$ the Reynolds number defined as $v_m r_m/\nu$.

In terms of these dimensionless quantities the steady-state equations of motion are:

$$\partial RU/\partial R + \partial RW/\partial Z = 0 \qquad (3)$$

$$U\partial U/\partial R + W\partial U/\partial Z - V^2R = -\partial P/\partial R + K[\partial^2U/\partial R^2 + (1/R)\partial U/\partial R - U/R^2 + \partial^2U/\partial Z^2] \qquad (4)$$

$$U\partial V/\partial R + W\partial V/\partial Z + UV/R = K[\partial^2V/\partial R^2 + (1/R)\partial V/\partial R - V/R^2 + \partial^2V/\partial Z^2] \qquad (5)$$

$$U\partial W/\partial R + W\partial W/\partial Z = -\partial P/\partial Z + K[\partial^2 W/\partial R^2 + (1/R)\partial W/\partial R + \partial^2 W/\partial Z^2]. \quad (6)$$

The dimensionless stream function ψ is introduced so that the continuity Equation (3) is satisfied:

$$U = -(1/R)\partial\psi/\partial Z; \; W = (1/R)\partial\psi/\partial R \quad (7)$$

The number of dependent variables may be reduced by eliminating the pressure by cross-differentiation of Equations (4) and (6) and subtraction to yield the vorticity transport equation:

$$R^2\{\partial[(\phi/R)\partial\psi/\partial R]/\partial Z - \partial[(\phi/R)\partial\psi/\partial Z]/\partial R\} - \{\partial[R^3\partial K(\phi/R)/\partial Z]/\partial Z + \partial[R^3\partial K(\phi/R)/\partial R]/\partial R\} - R\partial V^2/\partial Z = 0 \quad (8)$$

where the dimensionless vorticity ϕ has been defined as

$$\phi = \partial U/\partial Z - \partial W/\partial R \quad (9)$$

The stream function is then related to the vorticity through the equation:

$$-\{\partial[(1/R)\partial\psi/\partial Z]/\partial Z + \partial[(1/R)\partial\psi/\partial R]/\partial R\} - \phi = 0 \quad (10)$$

The equation of dimensionless circulation Γ defined as RV may be derived from the tangential momentum equation, Equation (5), and written in the form:

$$\{\partial(\Gamma\partial\psi/\partial R)/\partial Z - \partial(\Gamma\partial\psi/\partial Z)/\partial R\} - \{\partial[KR^3\partial(\Gamma/R^2)/\partial Z]/\partial Z + \partial[KR^3\partial(\Gamma/R^2)/\partial R]/dR\} = 0 \quad (11)$$

The vorticity, circulation and stream function equations (Equations (8), (11), and (10), respectively) are the governing equations for the problem. Their similarity can easily be observed; that is, each fits the general elliptic equation:

$$a\{\partial(\theta\partial\psi/\partial R)/\partial Z - \partial(\theta\partial\psi/\partial Z)/\partial R\} - \{\partial(b\partial c\theta/\partial Z)/\partial Z + \partial(b\partial c\theta/\partial R)/\partial R\} + d = 0 \quad (12)$$

Table 1. *Functions a, b, c and d*

θ	a	b	c	d
ϕ/R	R^2	R^3	K	$-R\partial V^2/\partial Z$
Γ	1	KR^3	$1/R^2$	0
ψ	0	$1/R$	1	$-\phi$

where θ is taken as the dependent variable and a, b, c and d are taken as standing for various functions. Table 1 above summarizes these functions.

Integration of elliptical differential equations requires conditions of variables on all field boundaries specified. These conditions are described below.

3. Boundary conditions

The boundary conditions to be imposed on the solution of equations of motion in terms of dimensionless velocities are:

At $Z = 0$, any R: $U = 0$ (13a)

$V = 0$ (13b)

$W = 0$ (13b)

At $Z = Z^+$, any R: $U = 0$ (14a)

$V = (1.4/R)[1 - \exp(-1.25R^2)]$ (14b)

$\partial W/\partial Z = 0$ (14c)

At $R = 0$, any Z: $\partial U/\partial R = 0$ (15a)

$V = 0$ (15b)

$\partial W/\partial R = 0$ (15c)

At $R = R^+$, any Z: $\partial U/\partial R = 0$ (16a)

$V = 1.4/R$ (16b)

$W = 0$ (16c)

Equations (14) above represent the assumption that a maintained two-dimensional Rankine vortex of Equation (2), is imposed on the upper boundary, and Equations (13), (15) and (16) imply physical continuity at the ground surface, axisymmetrical flow, and two-dimensionality of flow at large radius, respectively.

The following corresponding boundary conditions in terms of vorticity, stream function and circulation can be derived in a straightforward manner from Equations (13) and (16):

$$\text{At } Z = 0\text{: } \psi = 0 \tag{18b}$$

$$\Gamma = 0 \tag{18c}$$

$$\text{At } Z = Z^{+}\text{: } \phi/R = -(1/R^2)(\partial^2\psi/\partial^2 Z + \partial^2\psi/\partial R^2) + (1/R^3)\,\partial\psi/\partial R \tag{19a}$$

$$\partial\psi/\partial Z = 0 \tag{19b}$$

$$\Gamma = 1.4[1 - \exp(-1.25R^2)] \tag{19c}$$

$$\text{At } R = 0\text{: } \psi = 0 \tag{20b}$$

$$\Gamma = 0 \tag{20c}$$

$$\text{At } R = R^{+}\text{: } \phi/R = -(1/R^2)(\partial^2\psi/\partial R^2 + \partial^2\psi/\partial z^2) \tag{21a}$$

$$\partial\psi/\partial R = 0 \tag{21b}$$

$$\Gamma = 1.4 \tag{21c}$$

However the vorticity boundary conditions at the axis of symmetry ($R = 0$) and ground surface ($Z = 0$), respectively, require special consideration.

At the vicinity of the axis of symmetry, stream function has an approximate expression of the form:

$$\psi = AR^2 + BR^4 \tag{22}$$

where A and B are constants for a fixed Z. Substitution of this expression of ψ into Equation (10) yields the following expression for the vorticity ϕ/R at the axis:

$$\phi/R = -8B \tag{23}$$

Equations (22) and (23) allow the vorticity at the axis $(\phi/R)_{R=0}$ evaluated from stream function values ψ_1 and ψ_2 at radii R_1 and R_2, respectively, thus:

$$(\phi/R)_{R=0} = 8(\psi_1 R_2^2 - \psi_2 R_1^2)/[R_1^2 R_2^2 (R_2^2 - R_1^2)] \tag{20a}$$

This equation constitutes the boundary condition for ϕ/R at the axis of symmetry, $R = 0$.

At the ground surface, ψ and $(\partial\psi/\partial R)$ are both zero from Equations (18b) and (18c); and the gradients in the direction R are much smaller than those in the normal direction, they may be neglected. In this case, integration of vorticity equation, Equation (8), yields the following expression for ϕ/R:

$$\phi/R = (AZ + B)/(KR) \tag{24}$$

where A and B are constants for a fixed R. Substitution of this expression of (ϕ/R) into Equation (10) yields an expression for ψ:

$$\psi = -R(AZ^3 + 3BZ^2)/(6K) \tag{25}$$

Let values of ψ and (ϕ/R) at Z equal to Z_1 be ψ_1 and $(\phi/R)_1$, respectively. $(\phi/R)_{Z=0}$ may be evaluated from Equations (24) and (25), thus:

$$(\phi/R)_{Z=0} = -3\psi_1/(R^2 Z_1^2) - (\phi/R)_1/2 \tag{18a}$$

This equation constitutes the boundary condition at the ground surface $Z = 0$.

Equations (18) through (21) are boundary conditions of vorticity, stream function and circulation for the problem.

4. Numerical integration procedure

For numerical integration of vorticity, stream function and circulation equations, Equations (8), (10) and (11), respectively, along with boundary conditions, Equations (18) through (21), the flow field of $0 < R < R^{+}$ and $0 < Z < Z^{+}$ is presented by a rectangular grid system on the R, Z plane with

$$R_{i+1} = R_i + \Delta R_i \quad [i = 1(1)20] \tag{26}$$

$$Z_{j+1} = Z_j + \Delta Z_j \quad [j = 1(1)20] \tag{27}$$

Values of R^{+} and Z^{+} have both been taken as 10; and non-uniform grid spacings as shown in Fig. 2 have been used. Closest grids are used in the region where the shear stresses vary most rapidly, i.e., near the ground surface and in the vortex core. All derivatives in the governing equations are replaced by finite differences involving the values of the dependent variables at the node points. The differential equations are then reduced to a set of algebraic equations. An upwind-difference scheme, which has been used by Spalding and his co-workers (see Gosman et al., 1969) in their studies of a number of different problems, has been adapted by us in this study.

As mentioned in Section 2 that Equations (8), (10) and (11) can be represented by the general elliptic equation, Equation (12), it is convenient to discuss the finite difference equation by reference to this general equation. With the upwind difference scheme, Equation (12) is written in the form:

$$\theta_{i,j} = C_{i+1,j}\theta_{i+1,j} + C_{i-1,j}\theta_{i-1,j} + C_{i,j+1}\theta_{i,j+1} + C_{i,j-1}\theta_{i,j-1} + D \quad (28)$$

where

$$C_{i+1,j} = (A_{i+1,j} + B_{i+1,j}c_{i+1,j})/E$$

$$C_{i-1,j} = (A_{i-1,j} + B_{i-1,j}c_{i+1,j})/E$$

$$C_{i,j+1} = (A_{i,j+1} + B_{i,j+1}c_{i,j+1})/E$$

$$C_{i,j-1} = (A_{i,j-1} + B_{i,j-1}c_{i,j-1})/E$$

$$D = -d_{i,j}(Z_{j+1} - Z_{j-1})(R_{i+1} - R_{i-1})R_i/4E$$

$$E = (A_{i+1,j} + A_{i-1,j} + A_{i,j+1} + A_{i,j-1}) + c_{i,j}(B_{i+1,j} + B_{i-1,j} + B_{i,j+1} + B_{i,j-1})$$

$$A_{i,j+1} = a_{i,j}\{(\psi_{i-1,j+1} + \psi_{i-1,j} - \psi_{i+1,j+1} - \psi_{i+1,j}) + |\psi_{i-1,j+1} + \psi_{i-1,j} - \psi_{i+1,j+1} - \psi_{i+1,j}|\}/8$$

$$A_{i,j-1} = a_{i,j}\{(\psi_{i+j,j-1} + \psi_{i+1,j} - \psi_{i-1,j-1} - \psi_{i-1,j}) + |\psi_{i+1,j-1} + \psi_{i+1,j} - \psi_{i-1,j-1} - \psi_{i-1,j}|\}/8$$

$$A_{i+1,j} = a_{i,j}(\psi_{i+1,j+1} + \psi_{i,j+1} - \psi_{i+1,j-1} - \psi_{i,j-1}) + |\psi_{i+1,j+1} + \psi_{i,j+1} - \psi_{i+1,j-1} - \psi_{i,j-1}|\}/8$$

$$A_{i-1,j} = a_{i,j}\{(\psi_{i-1,j-1} + \psi_{i,j-1} - \psi_{i-1,j+1} - \psi_{i,j+1}) + |\psi_{i-1,j-1} + \psi_{i,j-1} - \psi_{i-1,j+1} - \psi_{i,j+1}|\}/8$$

$$B_{i,j+1} = (b_{i,j+1} + b_{i,j}) \times R_i(R_{i+1} - R_{i-1})/[4(Z_{j+1} - Z_j)]$$

$$B_{i,j-1} = (b_{i,j-1} + b_{i,j}) \times R_i(R_{i+1} - R_{i-1})/[4(Z_j - Z_{j-1})]$$

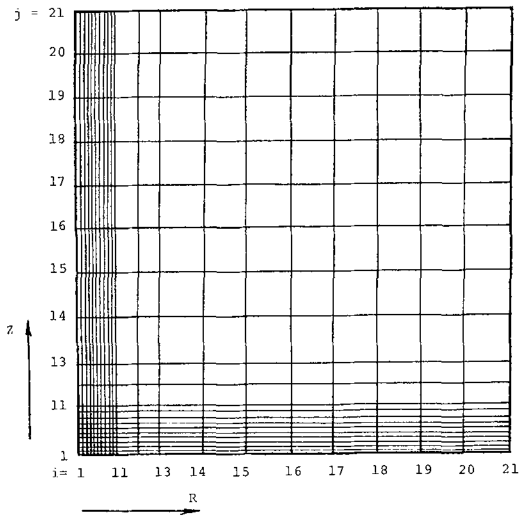

Fig. 2. Illustration of non-uniform grid system.

$$B_{i+1,j} = (b_{i+1,j} + b_{i,j})(Z_{j+1} - Z_{j-1}) \times (R_{i+1} + R_i)/[8(R_{i+1} - R_i)]$$

$$B_{i-1,j} = (b_{i-1,j} + b_{i,j})(Z_{j+1} - Z_{j-1}) \times (R_{i-1} + R_i)/[8(R_i - R_{i-1})] \quad (29)$$

θ in the above equations as mentioned previously stands for vorticity (ϕ/R), stream function (ψ), or circulation (Γ), dependent upon whichever is under consideration; and the functions a, b, c and d for each variable under consideration are given in Table 1.

The Gauss-Seidel's successive iteration method, e.g., see Ames (1965), is used to solve the set of algebraic equations, Equation (28). This method is based upon using the improved values immediately in computing the improvements for the next grid node. However, there are two kinds of boundary conditions, Equations (18) through (21); firstly, they are of constant values; and secondly, they are of the Gradient type. For the former, they are set at the initiation of the first iteration cycle and remain unchanged at successive iterations. For the latter, they are required to be improved at the end of each cycle, using the following algebraic equations which were derived from Equations (18) through (21):

At $Z=0$, (i.e., $j=1$) : $(\phi/R)_{i,1}$

$$= -3\psi_{i,2}/(R_i^2 Z_2^2) - (\phi/R)_{i,2}/2 \quad (30)$$

At $Z = 10$, (i.e., $j = 21$): $(\phi/R)_{i,21}$

$$= -\{2/R_i^2(R_{i+1} - R_{i-1})]\} \times [(\psi_{i+1,21} - \psi_{i,21})/(R_{i+1} - R_i) - (\psi_{i,21} - \psi_{i-1,21})/(R_i - R_{i-1})] - \{2/[R_i^2(Z_{20} - Z_{19})]\}[(\psi_{i,21} - \psi_{i,20})/(Z_{21} - Z_{20}) - (\psi_{i,21} - \psi_{1,19}) \times (Z_{21} - Z_{19})] + \{1/[R_i^3(R_{i+1} - R_{i-1})]\} \times [(\psi_{i+1,21} - \psi_{i,21})(R_i - R_{i-1})/(R_{i+1} - R_i) + (\psi_{i,21} - \psi_{i-1,21})(R_{i+1} - R_1)/(R_i - R_{i-1})] \quad (31)$$

At $Z = 10$, (i.e., j $= 21$) : $(\phi/R)_{i,21} = (\phi/R)_{i,20}$ (31)

$$\psi_{i,21} = \psi_{i,20} \quad (32)$$

At $R = 0$, (i.e., $i = 1$): $(\phi/R)_{i,j}$

$$= 8(\psi_{2,j} R_3^2 - \psi_{3,j} R_2^2)/[R_2^2 R_3^2(R_3^2 - R_2^2)] \quad (33)$$

At $R = 10$, (i.e., $i = 21$) : $(\phi/R_{21,j}$

$$= -\{2/[R_{21}^2(R_{20} - R_{21})]\}[(\psi_{21,j} - \psi_{20,j})/(R_{21} - R_{20}) - (\psi_{21,j} - \psi_{19,j})/(R_{21} - R_{19})] - \{2/[R_{21}^2(Z_{j+1} - Z_{j-1})]\} \times [(\psi_{21,j+1}\psi_{21,j})/(Z_{j+1} - Z_j) - (\psi_{21,j} - \psi_{21,j-1})/(Z_j - Z_{j-1})] \quad (34)$$

$$\psi_{21,j} = \psi_{20,j} \quad (35)$$

5. Computer program

A computer program in Fortran IV Language has been written to solve the algebraic Equations (28) through (35) using the iteration method mentioned above. Before iteration starts initial values are set: all the variables at the interior nodes are set to zero, the fixed boundary values are calculated by Equations (18) through (21), and the variable boundary values are calculated by Equations (30) through (35). The first iteration cycle is then initiated. Each iteration cycle is subdivided into three subcycles in the order of (ϕ/R), ψ and Γ calculations. In each subcycle calculation begins at the 20th column of the nodes (i.e., $i = 20$) with $j = 20(-1)2$, then the node values at the 19th, 18th columns and so on are calculated, until the 2nd column has been reached. Finally the boundary values are updated, using Equations (30) through (35), before the next subcycle starts. The above iteration cycle is then repeated until a preset convergence criterion (e.g., for this investigation all θ's for successive iteration agreeing within 0.1% as the criterion) is met.

At the end of the iteration process, values of (ϕ/R), ψ and Γ at grid nodes are stored followed by recovery of nondimensional velocities U and W from definition of ψ, V from definition of Γ, and dimensionless vorticity ϕ from ϕ/R. The dimensionless pressure defined as $(P_0 - P)$, where P_0 is the value of P at $Z = 0$, $R = R^+$, are then recovered through integration of momentum equations, Equations (4) and (6).

For the program output, the contours of the dimensionless stream function ψ, vorticity ϕ and pressure $(P_0 - P)$, respectively, are generated by a COMSAT CONTOUR ROUTINE and plotted using a CALCOMP plotter. The CALCOMP plotter is also used to plot the dimensionless velocity components, U and V at several radii versus Z and W at several heights versus R.

6. Results and discussions

Several runs with Reynolds number, N ranging from 1 to 2 000 have been made for the program in IBM 360 and CDC 6 600 machines. A typical computation for each Reynolds number takes from 8 to 15 minutes of IBM time and 1 to 2 minutes of CDC time. As an example, the computed results for Re $= 1\,000$ are presented and discussed below:

Figs. 3, 4 and 5 show the contour plottings of the dimensionless stream function ψ, vorticity ϕ, and pressure $(P_0 - P)$ distributions, respectively. The dimensionless radial velocity U and tangential velocity V are plotted versus height Z at several radii R in Figs. 6 and 7. The vertical velocity W is plotted versus R at several Z in Fig. 8.

Several interesting boundary-layer characteristics are observed from these figures. For the region far above the ground and outside the vortex core, i.e., at large Z and R, tangential velocity, as can be seen in the velocity diagrams Figs. 6, 7 and 8, dominates; the balance of force for this region is therefore characterized by a balance of the radial pressure gradient, see Fig. 5, and the centrifugal force. Near the ground surface, the retardation of the tangential velocity is seen in Fig. 7. This retardation is accompanied by a reduction of centrifugal force, the balance of pressure and centrifugal forces is thereby destroyed. The flow in this region is then characterized by the entrainment of flow to the boundary-layer as indicated by the deflection of stream lines toward the ground surface (Fig. 3), the large induced radial velocity U (Fig. 6), and the induced downward flow (negative W of Fig. 8). The eventual eruption of the entrained boundary-layer-flows at the vortex core root can be seen in Fig. 3 of the large radial gradient of stream function and in Fig. 8 of large updraft W. In addition the strong viscous effect in the region of the vortex core root is observed in Fig. 4 of the large magnitude of vorticity values in that region. The damaging effect on ground structures due to high vacuum in the region of the vortex core has often been mentioned in literature; it can be seen in Fig. 5 of the calculated $(P_0 - P)$ that this value ranges from 1 to 1.75 in the region of the vortex core root. For v_m of order of 100 m/sec, it corresponds to a pressure drop of 0.14 to 0.24 atmosphere. These values compare with the observed tornado physical parameters compiled by Ying & Chang (1969) of order of 0.1 atmosphere.

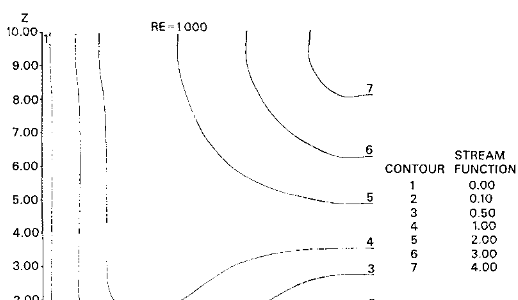

Fig. 3. Predicted dimensionless contour stream function, ψ.

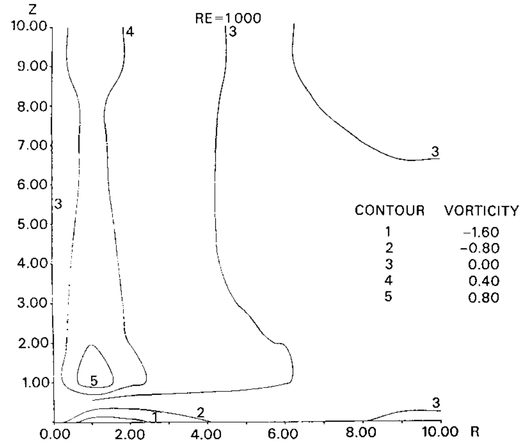

Fig. 4. Predicted dimensionless contour vorticity, ϕ.

Finally, it should be mentioned that no instruments have survived to obtain comprehensive data for the comparison with the present theory. Excellent laboratory experiments of Turner (1966) and Ying & Chang (1969) have, however, shown qualitatively the main features of flow characteristics near the ground surface. Fig. 9 shows vertical velocity profile measured by Turner (1966), and Figs. 10 and 11 show the radial and rangential velocity profiles, respectively, measured by Ying & Chang (1969). Qualitative similarity between the experimental velocity profiles, Figs. 10, 11 and 9, and the present theoretical results, Figs. 6, 7 and 8, can be observed. In particular it is noticeable that the Bödewadt type oscillatory U

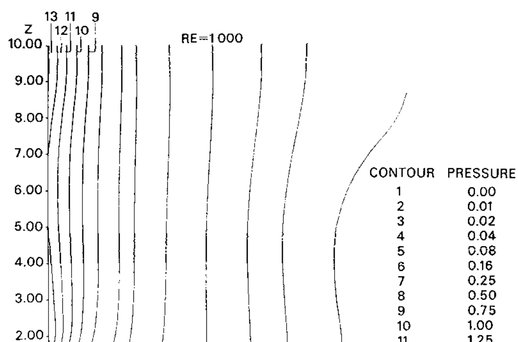

Fig. 5. Predicted dimensionless pressure, $(P_0 - P)$.

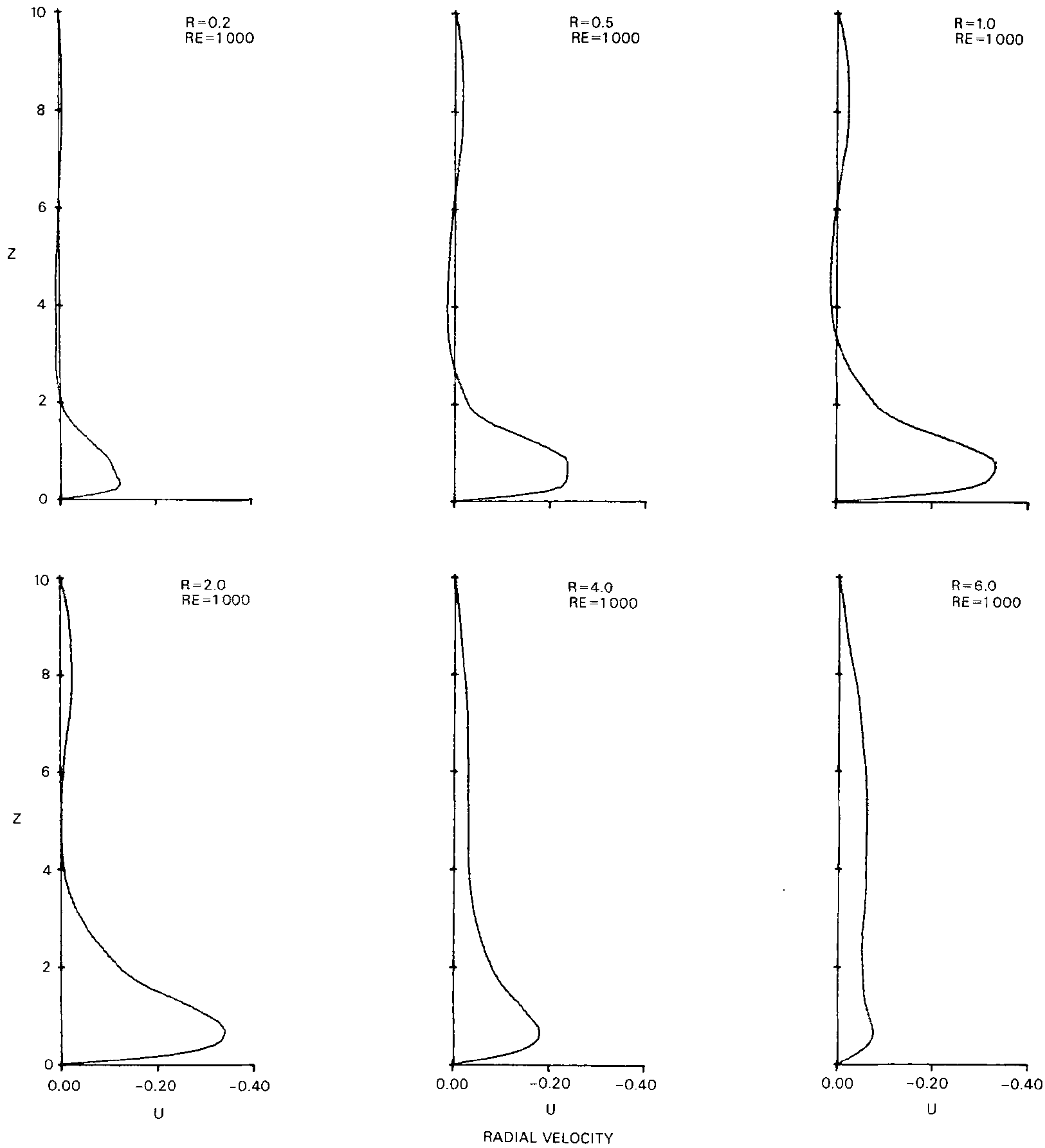

Fig. 6. Predicted dimensionless radial velocity U versus Z at several R's.

and V distributions at inner region and the change of flow direction for W (i.e., updraft at inner region and downdraft at outer region) are present in the theoretical as well as the experimental data.

7. Summary and conclusions

The three-dimensional boundary-layer beneath a maintained axisymmetrical intensive vortex has been investigated theoretically. The main assumptions have been the imposition of a Rankine-type intense vortex at the upper boundary and the uniform effective viscosity. Equations of motion in terms of dimensionless vorticity, stream function and circulation have been derived and generalized. A finite difference technique based upon upwind difference scheme and Gauss-Seidel's iteration procedure has been used to solve these equations. The method is

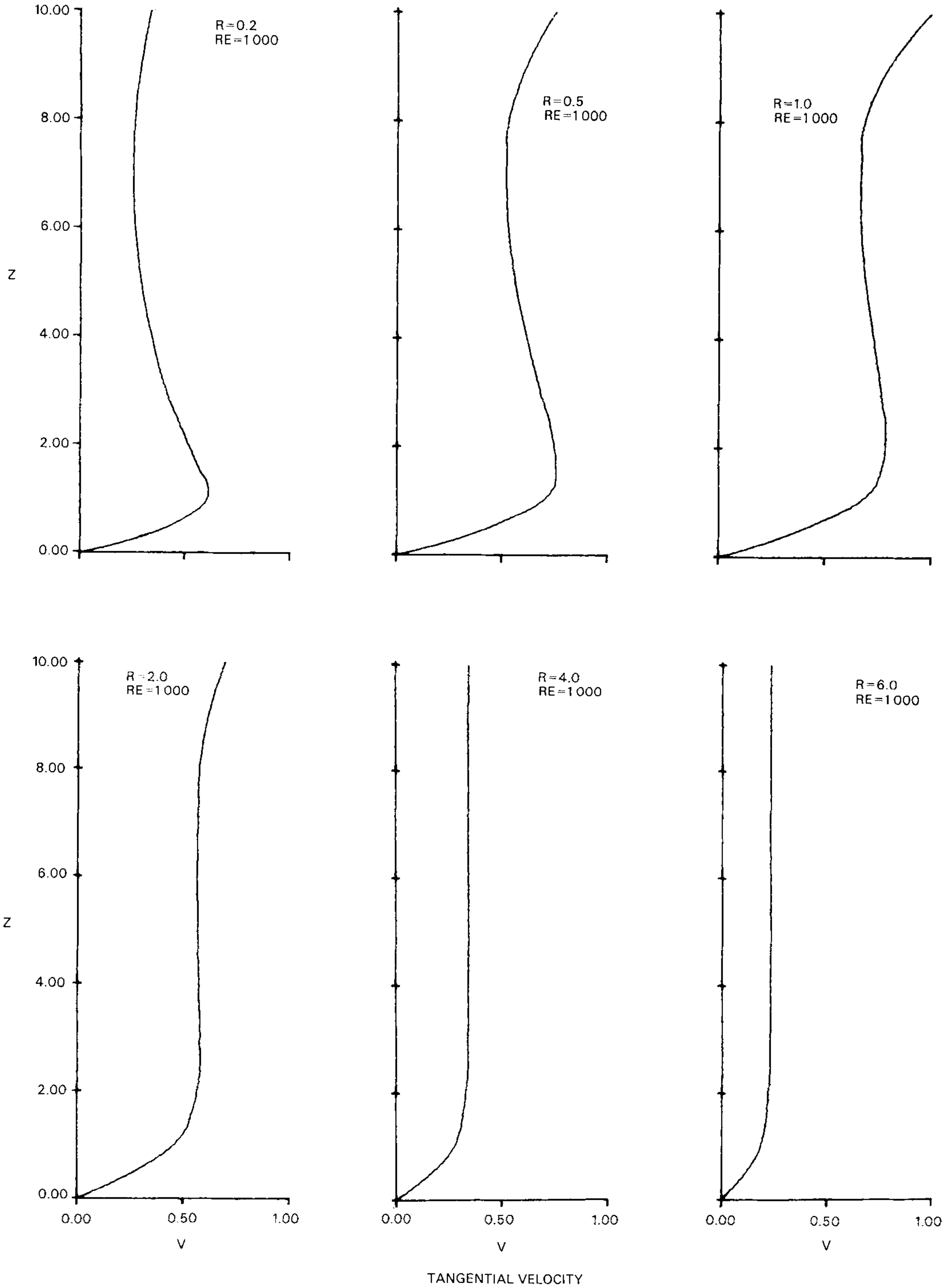

Fig. 7. Predicted dimensionless tangential velocity V versus Z at several R's.

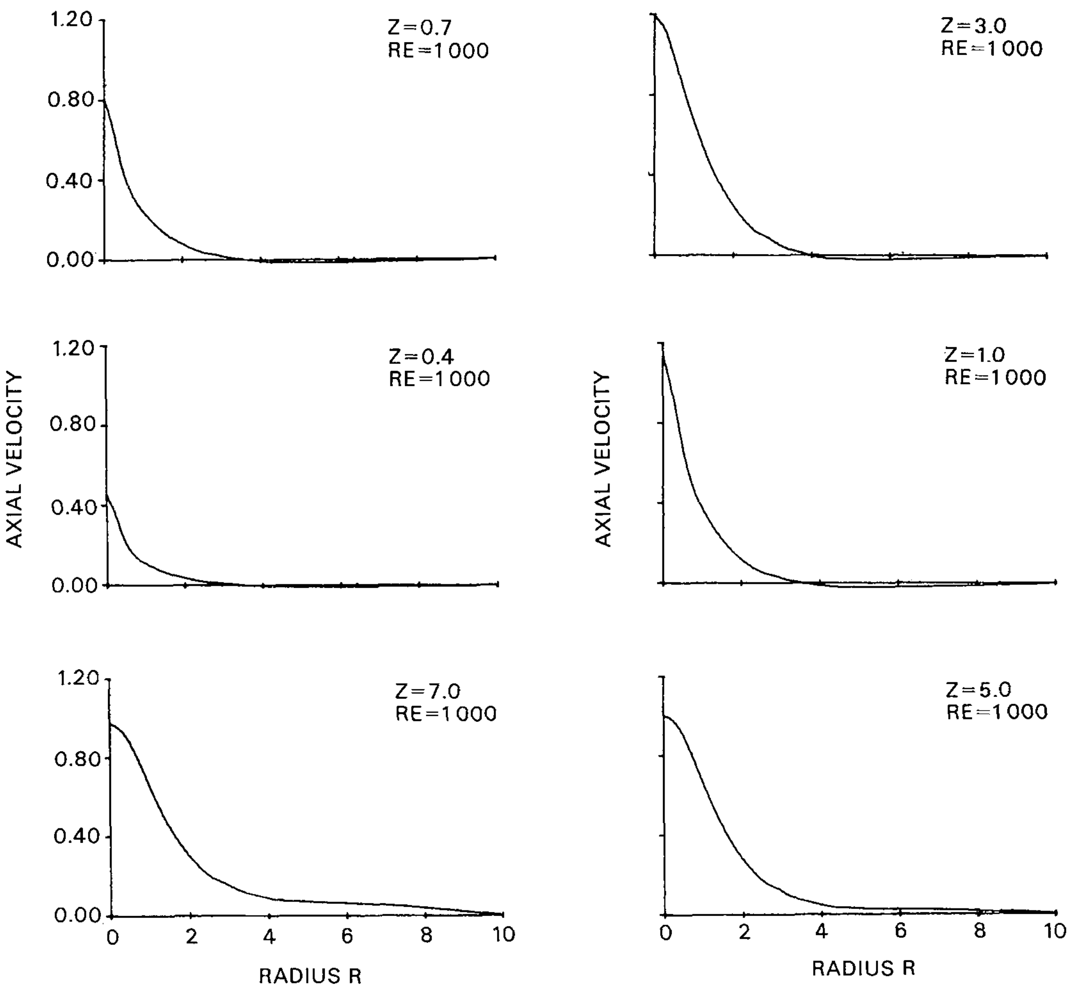

Fig. 8. Predicted dimensionless vertical velocity W versus R at several Z's.

found stable in the range of Reynolds numbers for the natural tornado. For each run, it takes 8 to 15 minutes of IBM 360-50 time and 1 to 2 minutes of CDC 6 600 time. In the absence of the measured data for the natural tornado, it is not possible to make quantitative comparison of the present calculations. However, the theoretical calculation predicts all the known qualitative characteristics of the three-dimensional boundary layer of intense vortices.

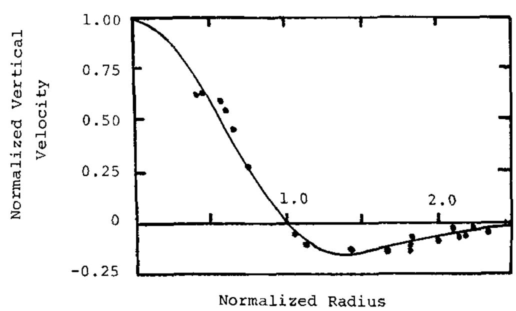

Fig. 9. Vertical velocity profile measured by Turner (1966).

8. Acknowledgement

This work was supported by the National Science Foundation under Grant GK-41469 and the Committee on Research of the George Washington University. The authors wish to express their appreciation to the Foundation and the Committee.

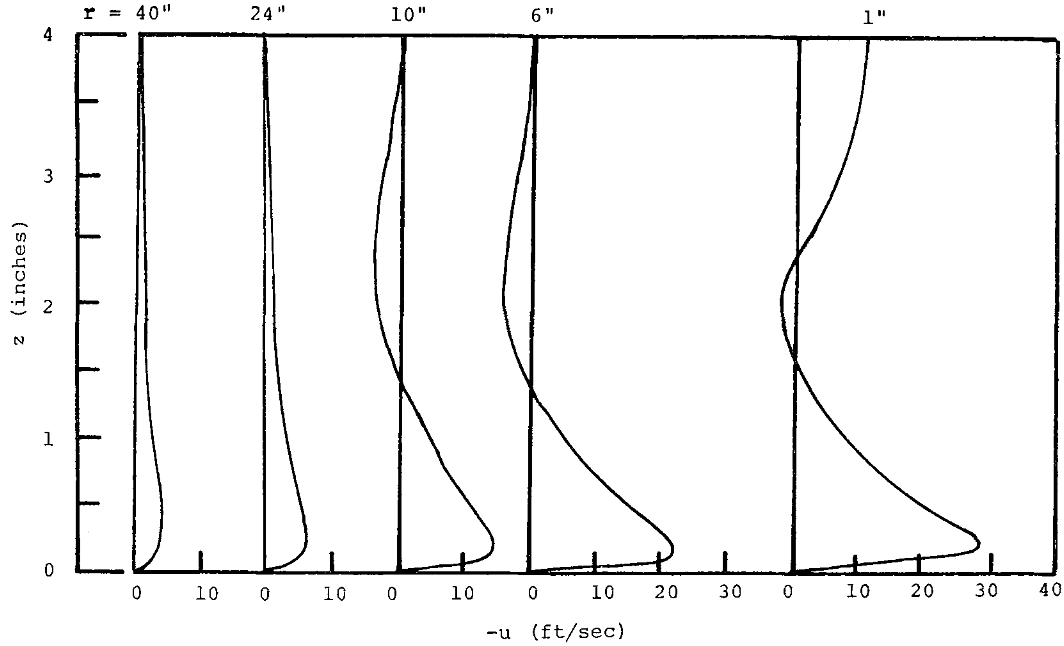

Fig. 10. Radial velocity profile measured by Ying & Chang (1969).

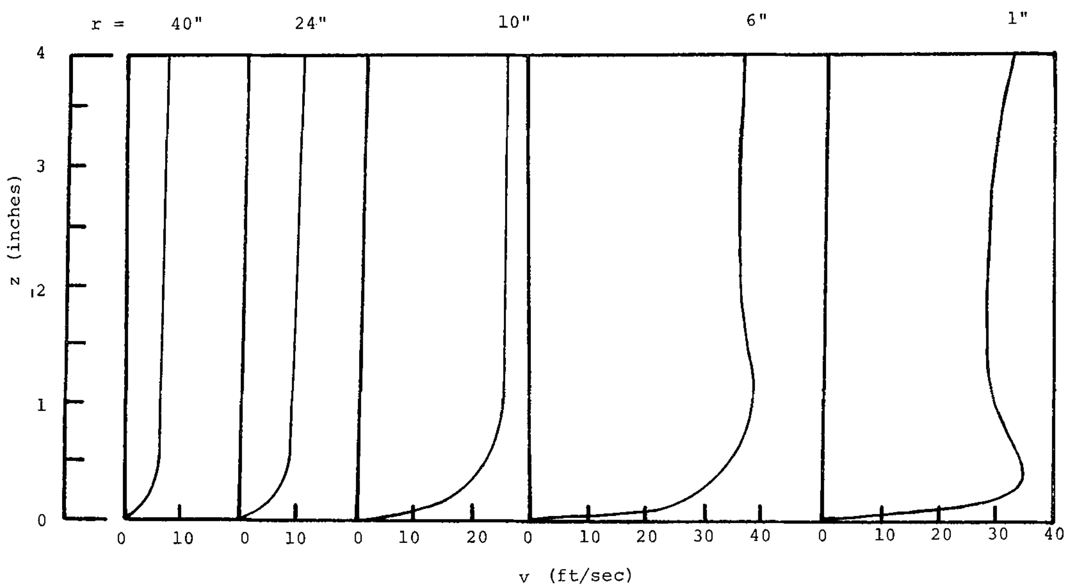

Fig. 11. Tangential velocity profile measured by Ying & Chang (1969).

REFERENCES

Ames, W. F. 1956. *Nonlinear partial differential equations in engineering*. Academic Press, New York.

Anderson, O. L. 1961. Theoretical solutions for the secondary flow in the end wall of a vortex tube. United Aircraft Corp., Report No. R-2494-I.

Bödewadt, W. T. 1940. Die Drehströmung über festem Grunde. *ZAMM 20*, 241–253.

Gosman, A. D, Pun, W. M., Runchal, A. K., Spalding, D. B. & Wolfstein, M. 1969. *Heat and mass transfer in recirculating flow.* Academic Press, New York.

Mack, L. M. 1962. The laminar boundary layer on a disk of finite radius in a rotating flow. Jet Propulsion Laboratory, Report No. 32–224.

Mack, L. M. 1964. The laminar boundary layer on a rotating disk of finite radius in a rotating flow. JPL Research Summary, No. 36–14, pp. 103–106.

Rott, N. & Lewellen, W. S. 1964. Boundary layers in rotating flows. Aerospace Corporation, Report No. ATN-64(9227)-6.

Schultz-Grunow, F. 1935. Der Reibungswiderstand rotierender Scheiben in Gehäusen. *ZAM*$_1$ *15*, 191.

Stewartson, K. 1957. On rotating laminar boundary layers. In *Proceedings of Symposium on Boundary Layer Research*, pp. 59–71. Springer-Verlag, Berlin.

Taylor, G. I. 1950. The boundary layer in the converging nozzle of a swirl atomizer. *Quarterly Journal of Mechanical and Applied Mathematics 3*, 129–139.

Turner, J. S. 1966. The constraints imposed on tornado-like vortices by top and bottom boundary conditions. *Journal of Fluid Mechanics 25*, 377–400.

Weber, M. E. 1956. Boundary layer inside a conical surface due to swirl. *Journal of Applied Mechanics 23*, 587–592.

Ying, S. J. & Chang, C. C. 1970. Exploratory model study of tornado-like vortex dynamics. *Journal Atm. Sci. 27*, 3–14.

ЧИСЛЕННОЕ МОДЕЛИРОВАНИЕ ТРЕХМЕРНЫХ ТЕЧЕНИЙ В ПОГРАНИЧНОМ СЛОЕ ПОДДЕРЖИВАЕМОГО ОСЕСИММЕТРИЧНОГО ВИХРЯ

С помощью численного моделирования изучается трехмерное течение в приземном пограничном слое под интенсивным вихрем Рэнкина. Выводятся и обобщаются уравнения движения для безразмерных завихренности, функции тока и циркуляции. Вместо схемы центральных разностей использовалась схема с шагом в направлении против ветра. Найдено, что метод является устойчивым в интервале чисел Рейнольдса, характерных для естественных торнадо. Результаты расчетов предсказывают известные физические характеристики трехмерных пограничных слоев интенсивных вихрей, а именно: распределение горизонтальных скоростей по вертикали во внешней области вихря является осциллирующим, движение в области ядра направлено вверх, в то время как во внешней области существует слабое нисходящее движение. Предсказываемое распределение давления также находится в пределах величин, наблюдаемых для реальных торнадо.